

Document downloaded from:

<http://hdl.handle.net/10251/212246>

This paper must be cited as:

García-Baldoví, A.; Del Angel, R.; Mouchaham, G.; Liu, S.; Fan, D.; Maurin, G.; Navalón Oltra, S.... (2023). Active site imprinting on Ti oxocluster metal-organic frameworks for photocatalytic hydrogen release from formic acid. *Energy & Environmental Science*. 16(1):167-177. <https://doi.org/10.1039/d2ee02258c>



The final publication is available at

<https://doi.org/10.1039/d2ee02258c>

Copyright The Royal Society of Chemistry

Additional Information

# Active site imprinting on Ti oxocluster metal-organic framework for the photocatalytic hydrogen release from formic acid

Alberto García-Baldoví,<sup>a</sup> Raquel Del Angel,<sup>b</sup> Georges Mouchaham,<sup>b</sup> Shanping Liu,<sup>c</sup> Dong Fan,<sup>c</sup> Guillaume Maurin,<sup>c</sup> Sergio Navalón,<sup>d</sup> Christian Serre,<sup>b\*</sup> Hermenegildo Garcia,<sup>a\*</sup>

<sup>a</sup> Instituto Universitario de Tecnología Química, Consejo Superior de Investigaciones Científicas-Universitat Politècnica de València, Universitat Politècnica de Valencia, Av. De los Naranjos s/n, 46023 Valencia, Spain

<sup>b</sup> Institut des Matériaux Poreux de Paris, Ecole Normale Supérieure, ESPCI Paris, CNRS, PSL University, Paris, France

<sup>c</sup> Institut Charles Gerhardt Montpellier UMR 5253 CNRS, Université de Montpellier, Place E. Bataillon, 34095, Montpellier Cedex 05, France

<sup>d</sup> Chemistry Department, Universitat Politècnica de València, Av. De los Naranjos s/n, 46023 Valencia, Spain

## Abstract

On-board hydrogen release from liquid organic carriers is a process that can make feasible the use of H<sub>2</sub> as transportation fuel. Formic acid is considered as one of the most convenient liquid hydrogen organic carriers, since it can be easily obtained from CO<sub>2</sub>, it is water soluble and it makes unnecessary to recover the H<sub>2</sub>-depleted byproducts. Compared

to the more conventional thermal catalytic decomposition of formic acid, the use of light in combination with a photocatalyst has been much less explored. Herein, we report a new paradigm in MOF photocatalysis that is the use of a microporous titanium oxocluster based metal-organic framework (Ti-MOF) endowed by formate-imprinted active sites, namely MIP-177\_LT (MIP stands for Materials from Institute of Porous Materials of Paris, LT for Low Temperature), as a highly efficient photocatalyst for H<sub>2</sub> release from formic acid without the need to neutralize acidity or the use sacrificial agents or noble metals. Noteworthy, a quantum efficiency of 22 % has been determined for the photocatalytic H<sub>2</sub> release that is highly remarkable for a non-toxic noble metal-free photocatalyst.

**Keywords:** Photocatalysis; liquid hydrogen organic carriers; on-board H<sub>2</sub> release from formic acid; imprinted MOFs as photocatalyst.

## Introduction

In the forthcoming decarbonized energy, hydrogen will play a key role as energy vector.<sup>[1]</sup> However, implementation of the hydrogen technology is hampered by several bottlenecks related to hydrogen generation from water using renewable energy, safe and adequate hydrogen storage and non-polluting hydrogen consumption. In the context of the use of hydrogen in transportation, one of the major problems is the low volumetric energy density of compressed hydrogen.<sup>[2]</sup> One approach to overcome this issue is the use of liquid organic compounds (known as *liquid organic hydrogen carriers*, LOHCs) that can release on-board hydrogen on demand.<sup>[3, 4]</sup> Among the requirements for an ideal LOHCs, the most important ones are easy synthesis, facile hydrogen release, lack of toxicity, water solubility and high percentage of hydrogen release. Thus, formic acid (HCOOH, FA) is among the most investigated LOHC not only owing to its hydrogen content (4.4 wt.%),<sup>[5]</sup> stability and non-toxic character, but also because its availability from biomass as well as from CO<sub>2</sub> hydrogenation. Besides, the HCOOH/CO<sub>2</sub> system can be considered as an ideal environmental-friendly system for hydrogen storage provided that CO<sub>2</sub> is obtained from air, in which case the whole hydrogen storage/hydrogen release cycle is CO<sub>2</sub> neutral. Indeed, dehydrogenation and re-hydrogenation reactions ( $\text{HCOOH} \leftrightarrow \text{H}_2 + \text{CO}_2$ ;  $\Delta G = -48.4 \text{ kJ mol}^{-1}$ )<sup>[6]</sup> can be considered as a neutral CO<sub>2</sub>-footprint cycle.<sup>[5]</sup>

Catalytic FA decomposition at room temperature has been reported using noble metals,<sup>[6-10]</sup> making the process of low applicability. Other transition metals can also promote hydrogen release from FA,<sup>[11-15]</sup> but they require some heating, occur at slower rate and are much less efficient. In addition, due to the known dissolution of metals in acid

medium and the ability of FA to form soluble metal-coordination complexes, corrosion of the catalyst and/or metal leaching are some of the limitations generally encountered in such a process.<sup>[16]</sup> To circumvent this issue, hydrogen release measurements have been reported for formate salts,<sup>[17]</sup> but this makes again the process less attractive since no FA is directly used, but a derivative containing unwanted alkali metal ions or other charge compensating cations, such as  $\text{NH}_4^+$ . This makes necessary FA neutralization with bases.<sup>[18]</sup> Moreover, other common problem of FA decomposition is the occurrence in some degree of FA dehydration ( $\text{HCOOH} \leftrightarrow \text{H}_2\text{O} + \text{CO}$ ;  $\Delta G = - 28.5 \text{ kJ mol}^{-1}$ ) taking place in some extent concomitantly with FA dehydrogenation.<sup>[19]</sup> It appears that the monodentate binding mode of FA on the catalyst surface at the expense of bridging mode adsorption is more favorable for the unwanted dehydration reaction.<sup>[6]</sup> The presence of CO from FA dehydration, even in minute proportions, is highly detrimental for the use of the released  $\text{H}_2$  in fuel cells, due to catalyst poisoning.<sup>[20]</sup> Therefore, a proper design of the active site to reach highly selective dehydrogenation reaction is desirable.

One alternative to conventional thermal catalysis that has been considerably less explored is the photocatalytic FA decomposition. Photocatalysis can promote FA decarboxylation.<sup>[21]</sup> In a general reaction mechanism, photogenerated holes abstract one electron from formic acid or formate giving  $\text{HCOO}\cdot$  radical that decomposes spontaneously, giving a  $\text{CO}_2$  molecule and a hydrogen atom.<sup>[21]</sup> Photogenerated electrons are consumed by  $\text{H}^+$  forming another hydrogen atom. Typical photocatalysts for FA decomposition are  $\text{TiO}_2$  materials in various crystalline phases, structural morphologies and dopants.<sup>[22-25]</sup> However, even when using  $\text{TiO}_2$  as photocatalyst, noble metal co-catalysts such as Pt<sup>[26, 27]</sup>, Au<sup>[23, 25]</sup>

and Pd <sup>[28]</sup> are generally employed to increase charge separation and to favor the occurrence of chemical reactions. Although much less studied, other photocatalysts besides TiO<sub>2</sub>, either independently or as heterojunctions, have also been tested for the photocatalytic FA decomposition.<sup>[21]</sup> The list includes toxic CdS <sup>[29]</sup> or metal phosphides prepared using poisonous and hazardous phosphine,<sup>[30]</sup> as well as BiVO<sub>4</sub>,<sup>[31]</sup> reduced graphene oxide<sup>[32-34]</sup> and carbon nitride.<sup>[35]</sup> Also in these cases, these photocatalysts contain in most cases noble metals to enhance their catalytic activity.

Metal-organic frameworks (MOFs) are becoming very attractive candidates for catalysis in general and, for photocatalysis in particular.<sup>[36-38]</sup> Thanks to the versatility of their hybrid (organic/inorganic) porous and highly ordered (crystalline) structure, their features can be finely tuned to deliver great catalytic performance with a minimal energetic penalty. MOFs have also been employed as passive hosts of active CdS, plasmonic Au@Pd or In<sub>2</sub>S<sub>3</sub>/Co(salen) photocatalysts for FA decomposition,<sup>[39-41]</sup> observing in some cases the evolution of a significant CO proportion,<sup>[39, 41]</sup> whose presence is highly detrimental for the operation of hydrogen fuel cells. In these examples MOFs were acting as porous supports with a negligible intrinsic activity. However, as far as we know MOFs by themselves have not been yet considered as candidates for hydrogen release from FA in the absence of any sacrificial agent.

MOF synthesis is a very active area of research.<sup>[42, 43]</sup> As an example of the various synthetic approaches offered by MOFs, there is a current trend in MOF synthesis of using, besides the organic building units (multitopic ligands) required to connect the inorganic building units (IBU), other organic additives known as modulators.<sup>[42]</sup> These modulators are

competing during the MOF synthesis with the structural ligands in terms of coordination with the metal ions of the IBU, allowing a better control of the nucleation process and, hence, on the overall crystallinity of the resulting MOF sample. Beyond their impact over the crystallization process, these modulators can induce the formation of structural defects that could be beneficial to enhance the MOF activity in various applications, particularly in catalysis and photocatalysis, by promoting accessible active metal sites and charge carrier trapping sites, respectively.<sup>[44, 45]</sup>

Among the various modulators reported, monotopic carboxylic acids and particularly FA are some of the preferred agents.<sup>[46, 47]</sup> Depending on the MOF structure, the nature of the building units, and the synthetic conditions, the modulator can either (i) replace the structural linker, leading a ligand defective structure, and/or (ii) occupy a free position inherently not affecting the structuring ligands. In both cases, the modulators can play a role to create potential accessible active sites. It occurred to us that FA as modulator can also be positively used to “*imprint*” in the resulting MOF structure an active site for the photocatalytic FA decomposition in the photoresponsive MOFs.

In this regard, Ti-MOFs are a particularly attractive sub-class of materials of most relevance as photocatalyst candidates, owing to their IBU constituted of Ti metal ions known for their photophysical response and redox photoactivity.<sup>[48]</sup> While in general transition metals with incompletely filled d orbitals undergo a fast  $d \leftarrow d$  electronic relaxation of the excited states,  $d^0$  or  $d^{10}$  transition metals, like  $Ti^{4+}$  or  $Zn^{2+}$ , not having this deactivation pathway are photocatalytically more efficient.<sup>[48]</sup> Our hypothesis is that one of these Ti-MOFs, denoted MIP-177-LT,<sup>[49]</sup> prepared in FA as pure solvent under solvothermal

conditions should be particularly efficient for FA decomposition, due to the FA modulator templating during its synthesis.<sup>[49]</sup> MIP-177-LT with a robust 3D microporous structure of formula  $\text{Ti}_{12}\text{O}_{15}(\text{mdip})_3(\text{formate})_6$  (mdip: methylene di-isophthalate), is built up of  $\text{Ti}_{12}\text{O}_{15}$  oxoclusters as IBU, where the  $\text{Ti}^{\text{IV}}$  ions are connected by  $\mu_3$ -oxo bridges, carboxylate groups of different mdip ligands and formate groups as depicted in Fig. 1.<sup>[49]</sup> As shown in this Figure, there are two types of formate groups. Half of them (highlighted in green) are linking two adjacent equatorial Ti ions in each  $\text{Ti}_{12}$ -oxocluster, and they are accessible through channels running along the *c*-axis. A second half (highlighted in yellow) are bridging two adjacent  $\text{Ti}_{12}\text{O}_{15}$  clusters and they are not exposed to the micropores. MIP-177-LT exhibits also remarkable chemical stability, among the best MOFs, including stability against strong acids such concentrated HCl, sulfuric and nitric acids, *aqua regia* and even 6 M  $\text{H}_3\text{PO}_4$  which has been of interest for proton conductivity<sup>[50]</sup> or release of nitric oxide in simulated body fluid conditions.<sup>[51]</sup>

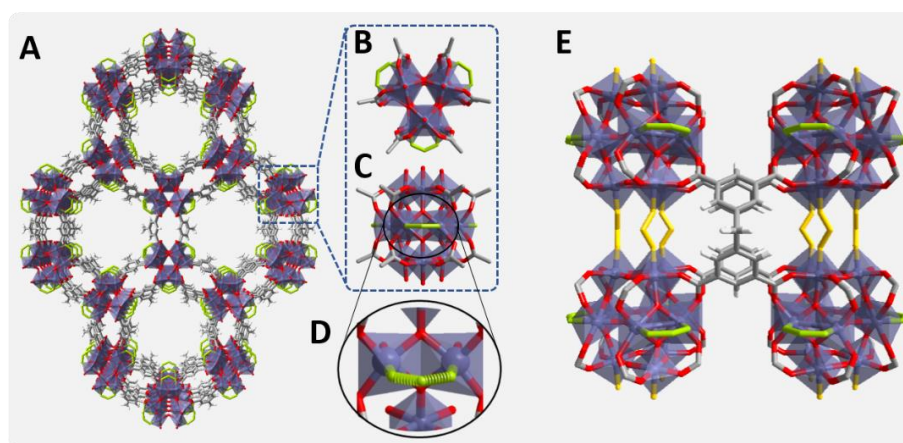


**Fig. 1.** **A**, Crystal structure of MIP-177-LT. **B** and **C**,  $\text{Ti}_{12}\text{O}_{15}$  cluster showing non-bridging formates (equatorial) in green, top and side view, respectively. **D**, View of the equatorial formate-imprinted sites. **E**, View showing in yellow the bridging formates between two adjacent  $\text{Ti}_{12}$  oxoclusters aligned along the *c*-axis. Taken with permission from ref. <sup>[49]</sup>.



Considering the remarkable photocatalytic activity of Ti-MOFs, the high chemical stability of MIP-177-LT to strong acids being prepared in formic acid at reflux temperature, it motivated us to consider this MOF as formate-*imprinted* catalyst to promote the photocatalytic hydrogen release from FA. Formate imprinting should make possible the recognition of FA by the active sites, fitting adequately in the structure. As it will be shown below, containing exclusively Ti as the only metal in the absence of noble metals, MIL-177-LT is a very efficient and stable photocatalyst for hydrogen release from aqueous solutions of FA, comparing favorably with other Ti- and Zr-containing MOFs and with conventional TiO<sub>2</sub> photocatalysts.

## **Results and discussion.**

The concept of the present study is summarized in Fig. 2 in which key aspects, like formate molecular imprinting, structural stability against strongly corrosive acids, the presence of Ti oxoclusters and other features of MIP-177-LT have been highlighted. The synthesis of MIP-177-LT was performed as reported <sup>[49]</sup> from Ti(*i*PrO)<sub>4</sub> as the molecular source of Ti<sup>IV</sup> and di(isophthalyl)methane (H<sub>4</sub>mdip) as linker in FA as solvent under solvothermal conditions (100-120 °C) during 3 days. MIP-177-LT synthesis is reliable and it can be up scaled up to 100 g. The samples used for the present study exhibit the expected PXRD pattern, chemical composition and spectroscopic properties as reported before.<sup>[49]</sup> Fig. 3 shows XRD characterization data of the MIP-177 sample under study. Besides the as-synthesized MIP-177-LT, another MIL-177-LT sample was submitted to acid treatment

(MIP-177-LT-AT), since this process removes formate units from the Ti sites, while increasing somewhat the specific surface area of the material that goes from 640 for MIP-177-LT to  $560 \text{ m}^2 \times \text{g}^{-1}$  for MIP-177-LT-AT. In addition, other difference between the two MOFs is the blue shift of the absorption onset wavelength in the diffuse reflectance UV-Vis absorption spectrum of MIP-177-LT-TA compared to MIP-177-LT (Fig. S1), probably due to the removal of oligomeric  $\text{TiO}_x$  impurities occupying some pore space that could be present in MIP-177-LT. Additional characterization, including diffuse-reflectance optical spectra, diffraction patterns, isothermal  $\text{N}_2$  and  $\text{CO}_2$  adsorption/desorption plots and SEM images of the MIP-177-LT and MMIP-177-LT-TA samples used in the present study, including particle morphology and XPS data are presented also in Fig. S1. For the sake of comparison, this study was also completed with MIL-125(Ti) and UiO-66(Zr) taken as reference MOF photocatalysts and commercial P25  $\text{TiO}_2$ .

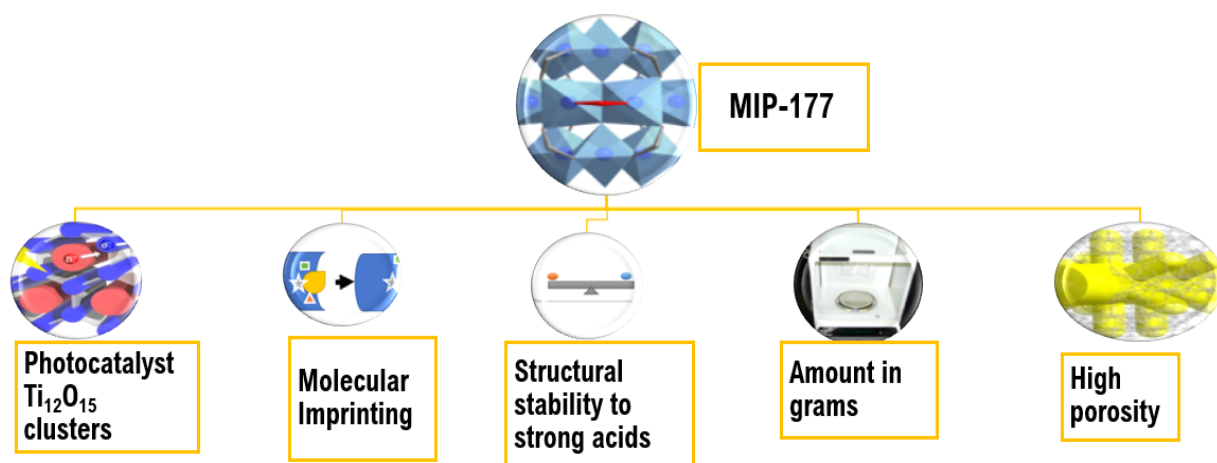


Fig. 2. MIP-177 features that make this material adequate as photocatalyst for  $\text{H}_2$  release from FA.

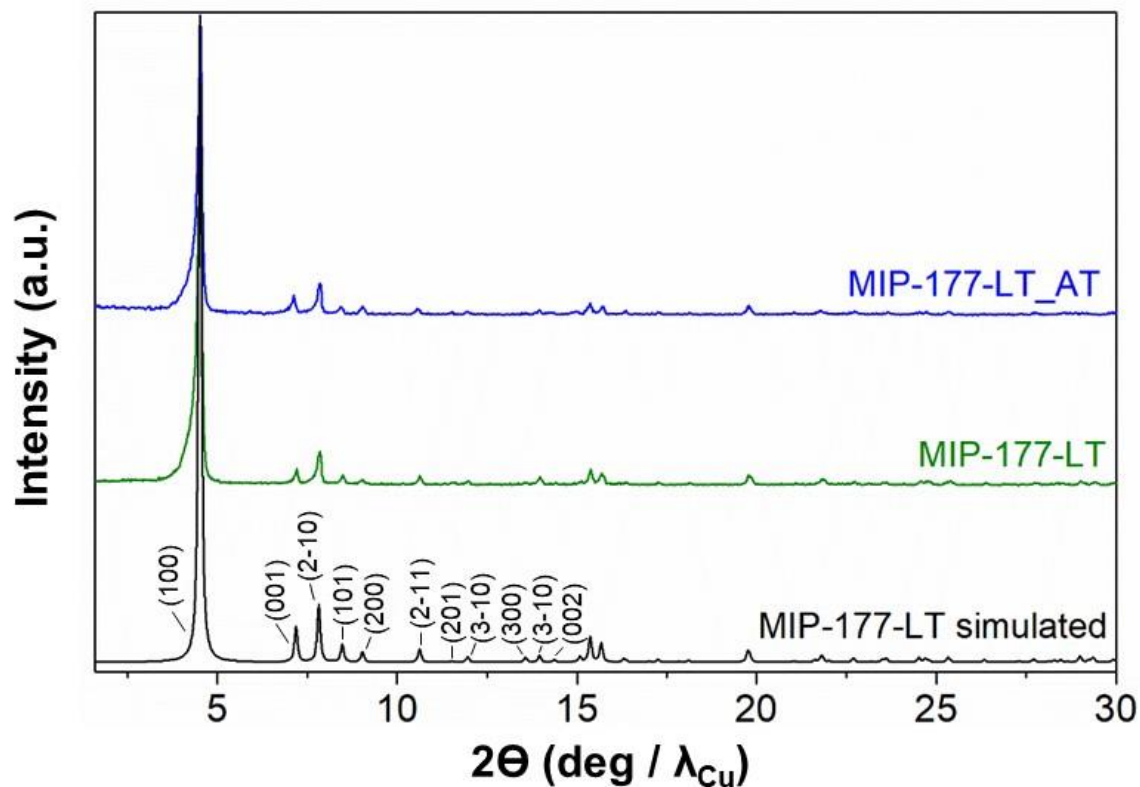


Fig. 3. PXRD patterns of the pristine and the acid treated (AT) MIP-177-LT samples, in comparison with the simulated one **in which the Miller indices have been indicated.**

#### Photocatalytic stability.

Prior to evaluation of the photocatalytic H<sub>2</sub> release from FA, blank controls irradiating MIP-177-LT and MIP-177-LT-AT photocatalysts were performed. These initial screening experiments serve to determine the photo stability of MIP-177-LT and MIP-177-LT-AT. Irradiations were carried out for 24 h periods as dry powders upon exposure to light of different wavelength regions. The results are summarized in Table S1. Previous reports in the literature have shown that carboxylate MOFs can undergo partial

photodecarboxylation under UV light in a significant extent of up to 33 % of the total carboxylate groups of the material during prolonged (months) irradiation times under UV-Vis light.<sup>[52]</sup>

In the present case, it was found that irradiation through Pyrex with the full spectral output of a 300 W Xe lamp for 24 h of 10 mg of MIP-177-LT gives rise to the evolution of 8  $\mu\text{mol}$   $\text{CO}_2$  accompanied with two-orders of magnitude lesser amounts of  $\text{H}_2$ . This  $\text{CO}_2$  evolution corresponds to about 8.8 % of the carboxylate groups present in the material according to its theoretical  $\text{Ti}_{12}\text{O}_{15}(\text{mdip})_3(\text{formate})_6$  formula. In comparison,  $\text{CO}_2$  evolution for the same period of time decreased by factors of 3.5 and 5.7 times less when the sample was irradiated with 360 and 400 nm cut-off filters, respectively. This correspond to the photochemical decomposition in 24 h of 2.5 and 1.5 % of the carboxylate groups present in the material according to the theoretical formula, meaning that short wavelengths from 300 to 360 nm are responsible for most (71 %) of the MIP-177-LT self-decomposition and that irradiation with wavelengths longer than 400 nm diminishes MIP-177-LT damage in a 91 %.

Similar photostability studies were also performed on MIP-177-LT-AT. The same general trend, but with even lesser  $\text{CO}_2$  evolution (maximum of 2.00  $\mu\text{mol}$  at 24 h) was observed. Incidentally, for MIP-177-LT-AT generation of  $\text{CH}_4$  in higher proportions than the minute  $\text{H}_2$  amounts was detected.

These preliminary studies indicate that deep UV radiation of wavelengths shorter than 360 nm is responsible for most of the  $\text{CO}_2$  evolution and that part of these gases

derives from species present inside the channels that can be removed by acid treatment, since MIP-177-LT-AT has 70 % lesser CO<sub>2</sub> and CH<sub>4</sub> evolution. This less-damaging spectral range correspond to the solar spectrum at the earth surface.

To put into context these CO<sub>2</sub> evolution values with those that will be reported below in FA decomposition, they are three orders of magnitude lower and in the case of H<sub>2</sub> even lower. Therefore, the conclusion of these preliminary control studies is that self-decomposition is not relevant compared to the photocatalytic FA decomposition activity data presented herein below.

#### *H<sub>2</sub> release from photocatalytic FA decomposition.*

Photocatalytic H<sub>2</sub> release from FA experiments were carried out at room temperature under continuous magnetic stirring of 10 mg of either MIP-177-LT or MIP-177-LT-AT in 15 mL of 10<sup>-3</sup> M FA solution in water in a closed 51 mL Pyrex reactor upon illumination of a 300 W Xe lamp (see Fig. S2). Gas evolution was periodically analyzed for 2 h irradiation runs by injecting the gases of the head space in a micro-GC. According to the dehydrogenation and dehydration reactions (eqs. 1 and 2), photocatalytic decomposition of FA can afford stoichiometric H<sub>2</sub> and CO<sub>2</sub> or stoichiometric H<sub>2</sub>O and CO, respectively. In agreement with the preliminary photo stability study, control experiments in the absence of FA under otherwise identical conditions or irradiation of FA in the absence of any MIP-177 photocatalysts show a negligible amount of H<sub>2</sub> compared to the large values observed for the FA solutions.

Noteworthy, the decomposition products observed in all the experiments in the presence of MIP-177 photocatalysts were predominantly H<sub>2</sub> and CO<sub>2</sub>, accompanied with much lesser amounts of CH<sub>4</sub>. Importantly, the amount of CO was below the detection limit of our GC analysis, corresponding to CO concentrations lower than 0.1 % in the gas composition, much smaller than the values about 10 % reported for TiO<sub>2</sub>.<sup>[21, 39]</sup> 7.0 μmol H<sub>2</sub>, corresponding to over 46 % of the theoretical stoichiometric amount for complete FA dehydrogenation (15 μmol) were quantified at 2 h of reaction time using fresh MIP-177-LT. Worth noting is that while H<sub>2</sub> evolution increased quite linearly with the irradiation time, CO<sub>2</sub> evolution was somewhat higher than expected according to H<sub>2</sub> at shorter irradiation times, but finally reached a quasi-stoichiometric amount. Fig. 4 A shows the temporal gas evolution measured for the fresh MIP-177-LT sample. Note that the continuous lines do not correspond to the fitting of the experimental points to a kinetic model. In accordance with the expected influence of acid washings removing impurities, the photocatalytic activity of the acid treated MIP-177-LT-AT was even better and exhibit almost complete FA decomposition in 2 h with quasi-stoichiometric amounts of H<sub>2</sub> (13.0 μmolg<sup>-1</sup>) and CO<sub>2</sub> at 2 h irradiation time (Fig. 4 B and 4 C). Also, some methane formation was observed for MIP-177-LT, while in comparison the presence of methane in the case of MIP-177-LT-AT as photocatalyst was barely detectable.

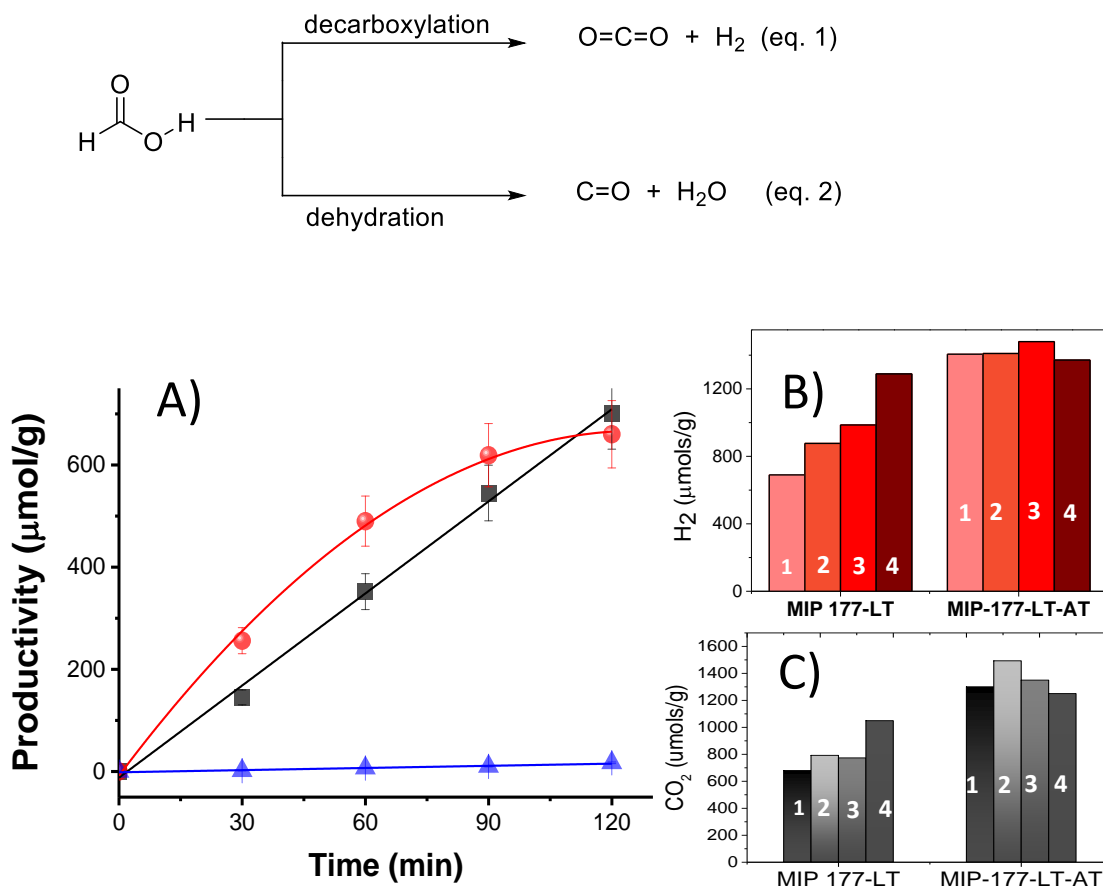


Fig. 4. A) Temporal profile of  $\text{H}_2$  (black),  $\text{CO}_2$  (red) and  $\text{CH}_4$  (blue) evolution upon UV-Vis irradiation of a  $10^{-3}$  M FA aqueous solution in the presence of MIP-177-LT as photocatalyst. **The continuous lines are not fittings to kinetic models.** B)  $\text{H}_2$  or  $\text{CO}_2$  (C) production at 2 h irradiation time in the presence of MIP-177-LT or MIP-177-LT-AT upon the reuse number as indicated in the drawing. Reaction conditions: photocatalyst 10 mg, solution volume 20 mL, FA concentration  $10^{-3}$  M, 300 W Xe lamp through Pyrex.

Powder XRD and XPS data of the MIP-177-LT samples after the photocatalytic FA decomposition did not reveal any change (Fig. S3), confirming the excellent stability of the materials under the reaction conditions, in good accordance with the reported stability of MIP-177-LT under strongly acidic conditions. **In addition, surface area measurement of the MIP-177-LT sample used as photocatalyst for  $\text{H}_2$  release and exhaustive washing with water**

indicates a surface area of ###  $\text{m}^2\text{g}^{-1}$  that is somewhat lower than the specific area of the fresh material, but in line with that of MIP-177-LT-AT confirming porosity stability. Similarly, SEM images of the used MIP-177-LT sample (Fig. S3) show some abrasion of the particles that otherwise maintain the crystalline morphology of the fresh MIP-177-LT material.

In agreement with the catalyst stability in FA, reusability tests provided an important observation in the case of MIP-177-LT, i.e.,  $\text{H}_2$  and  $\text{CO}_2$  evolution become faster and the final  $\text{H}_2$  amount evolved at 2 h reaction time continuously grows upon reuse as presented in Fig. 4 B. Thus, the final  $\text{H}_2$  amount increased from  $700 \mu\text{mol} \times \text{g}^{-1}$  to 877, 896 and  $1289 \mu\text{mol} \times \text{g}^{-1}$  for the first, second, third and fourth use, respectively. The  $\text{H}_2$  amount released in the fourth use is about 86 % of the maximum theoretical  $\text{H}_2$  amount according to the  $10^{-3} \text{ M}$  FA concentration. The apparent turnover frequency (TOF) obtained by dividing the evolved  $\text{H}_2$  mols by the mols of Ti atoms in the photocatalyst also grows from  $2.5 \times 10^{-2}$  to  $12.7 \times 10^{-2} \text{ h}^{-1}$  (see supporting information for details of apparent TOF calculation). As commented earlier and seen in Figure 4A, fresh MIP-177-LT samples evolve at initial times higher  $\text{CO}_2$  amounts than the corresponding stoichiometric  $\text{H}_2$  amount. In comparison, as the same MIP-177-LT sample is increasingly reused,  $\text{CO}_2$  evolution followed the same temporal profile as that  $\text{H}_2$  and the amounts of evolved  $\text{CO}_2$  and  $\text{H}_2$  in the fourth use were significantly higher than for the fresh MIP-177-LT sample. Therefore, the enhanced photocatalytic  $\text{CO}_2$  evolution observed for as-synthesized MIP-177-LT sample at initial reaction times is specific of this material and it tends to become corrected to the expected 1:1  $\text{CO}_2/\text{H}_2$  ratio upon extended irradiation. Furthermore, worth noting is that acid-treated MIP-177-LT-TA sample exhibits a 1:1  $\text{CO}_2/\text{H}_2$  evolution since the start of the irradiation,



meaning again that non-stoichiometric CO<sub>2</sub>/H<sub>2</sub> evolution is exclusive of fresh MIP-177-LT sample. Assuming that the charge separation state efficiency and other parameters related to the photocatalytic mechanisms dependent on the intrinsic electronic MIP-177-LT properties are constant upon reuse, TOF data indicate that about 5.1 more sites are becoming active upon MIP-177-LT reuse. This can be interpreted considering that only a fraction of the adjacent Ti atoms accessible from the pore space was initially available for the photocatalytic reaction in the fresh photocatalyst, and this percentage increases upon continuous irradiation, probably due to the decomposition of the structural formate groups bridging two equatorial Ti atoms of the same Ti<sub>12</sub> cluster. The factor of TOF enhancement about 5 upon reuse would indicate, then, that for the extensively used MIP-177-LT electrons and holes located at any of the six positions of equatorial bridging formates accessible from the micropores have become photocatalytically active upon extended use, increasing in this way by a factor of 5 the efficiency of charge separation in the generation of CO<sub>2</sub>/H<sub>2</sub>.

Notably, when considering the acid treated MIP-177-LT-AT that contains much less formates onto the Ti<sub>12</sub>O<sub>15</sub> oxocluster due to the acid treatment, the photocatalytic activity from the first to the fourth use becomes rather constant, although some increase in the TOF value from 0.35 h<sup>-1</sup> for the fresh sample to a TOF of 0.46 h<sup>-1</sup> for the fourth times used material was also observed. Most likely 0.46 h<sup>-1</sup> is about the maximum TOF value that can be achieved with the light power used in the present photocatalytic decomposition study. TOF values indicate that the performance of MIP-177-LT-AT is about four-fold higher than that of fresh MIP-177-LT, illustrating again the benefits of the acid treatment to achieve the

optimal photocatalytic activity. Interestingly, according to the stoichiometry of eq. 1 one can easily verify that a complete decomposition of all the FA present in the aqueous solution was achieved at 2 h irradiation for the MIP-177-LT-TA photocatalyst.

In addition, PXRD analysis after the five times used MIP-177-LT-AT sample did not reveal apparent change in the pattern compared to the fresh material (Fig. S4) again in accordance with the stability of MIP-177-LT in acid media.

### *Benchmarking.*

To put the photocatalytic activity of MIP-177-LT and MIP-177-LT-TA into context, similar experiments on the photocatalytic H<sub>2</sub> release by FA decomposition were performed using **the same mass of** other benchmark MOFs photocatalysts, namely, MIL-125(Ti) and UiO-66(Zr). As commented earlier, to our knowledge, there are no precedents in the literature on the use of MOFs as the active photocatalyst for the photocatalytic FA decomposition. As summarized in Table 1, H<sub>2</sub> evolution was also observed for these MOFs with a final H<sub>2</sub> production at 2 h of 260 and 360  $\mu\text{mol} \times \text{g}_{\text{photocatalyst}}^{-1}$  for MIL-125(Ti) and UiO-66(Zr), respectively. This represents one half or less the photocatalytic activity of fresh MIP-177-LT and about seven times lower than that of highest performing MIP-177-LT-TA. Note that out of a few disordered defects, MIL-125(Ti) does not contain any structural site with formate imprinting. UiO-66(Zr) exhibits ordered or disordered sites, depending on the synthesis conditions, that are likely to be accessible to formate anchoring, but it is based on a different coordination mode of the metal (Zr<sup>4+</sup> is 8 coordinated against 6-fold for Ti<sup>4+</sup> ions).

Considering the unique structure of MIP-177-LT, we attribute this strong catalytic enhancement to the effect of the formate imprinting in the structure due to the specific arrangement of Ti atoms in the cluster. In comparison, the photocatalytic activity of MIL-125(Ti) and UiO-66(Zr) must correspond to the general electron/hole activity of photogenerated charge separate state to decompose FA.<sup>[53]</sup>

To further support that formate imprinting of  $Ti_{12}O_{15}$  metal nodes in MIP-177-LT is responsible for this better performance in  $H_2$  release from FA, photocurrent measurements using the same mass of the three MOFs were conducted. The results are presented in Fig. S5. As it can be seen there, under the same conditions the photocurrent density of UiO-66 and MIL-125(Ti) was six and three times higher than that of MIP-177-LT, meaning that the photogenerated charge carriers that can be extracted from these MOFs are higher than in MIP-177-LT. In spite of this lower charge extraction, the photocatalytic activity for FA decomposition of MIP-177-LT is much higher, indicating that it is the special structure of the  $Ti_{12}O_{15}$  oxo clusters what favors FA decomposition in spite of the lesser number of holes.

Table 1. Relative photocatalytic activity of reference photocatalysts compared to MIP-177-LT. *Reaction conditions: FA concentration  $10^{-3}$  M, photocatalyst 10 mg, solution volume 15 mL, 300 W Xe lamp through Pyrex, reaction time 2 h.*

Photocatalysts	$H_2$ production ( $\mu\text{mols} \times g_{\text{photocatalyst}}^{-1}$ )	TOF ( $h^{-1}$ )
----------------	--	------------------

MIL-125(Ti)	266	0.021
UiO-66(Zr)	360	0.031
P-25 TiO <sub>2</sub>	340	0.009
MIP-177-LT-AT (fresh)	1300	0.35

To show a broader context, commercial P25 TiO<sub>2</sub> was finally evaluated as photocatalyst under the same conditions. Note that most of the studies with TiO<sub>2</sub> as photocatalyst use noble metal co-catalysts and herein the purpose was to evaluate the activity of plain TiO<sub>2</sub> that could be compared with the Ti<sub>12</sub>O<sub>15</sub> clusters of MIP-177-LT. The results presented in Table 1 show that P25 exhibits a H<sub>2</sub> production at 2 h irradiation time similar to that measured for UiO-66(Zr) and much lower than those of the formate *imprinted* MIP-177-LT that upon reuse can be almost an order of magnitude more active than P25 TiO<sub>2</sub>.

Furthermore, apparent activation energy values ( $E_a$ ) for the photocatalytic FA decomposition in the range of temperatures from 25 to 40 °C was determined for MIP-177-LT and TiO<sub>2</sub> as photocatalysts. The results are presented in Fig. S6 in supplementary material. The corresponding  $E_a$  values for MIP-177-LT and TiO<sub>2</sub> were 57.5 and 107.0 kJ × mol<sup>-1</sup>, respectively. We attribute the lower FA decomposition  $E_a$  to the favorable structure of the active site in MIP-177-LT.

### *Influence of FA concentration.*

To take benefit from the exceptional chemical stability of MIP-177-LT in strong acid media, additional photocatalytic measurements were carried out with FA concentrations of  $10^{-2}$  and 1 M using MIP-177-LT as reference photocatalyst. The results summarized in Table S2 show that the  $H_2$  evolution rate does not increase upon increasing FA concentration from  $10^{-3}$  to  $10^{-2}$  M. The highest concentration of 1 M, makes  $H_2$  evolution even slower than when the concentration is  $10^{-2}$  M. PXRD of the used MIP-177-LT samples after their use as photocatalysts showed no appreciable changes in the PXRD patterns. Chemical analysis of the FA solution revealed an increase in the Ti content as a function of FA concentration that is <0.001, 0.012 and 4.86 % of the total Ti content present in the fresh MIP-177-LT used as photocatalyst for  $10^{-3}$ ,  $10^{-2}$  and 1 M FA solutions, respectively.

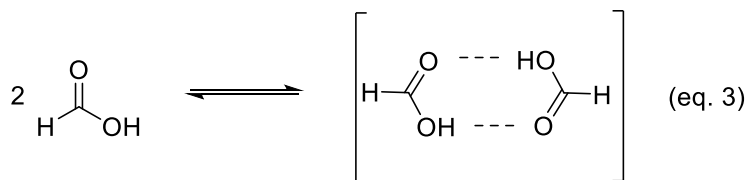
To understand the negative effect of excessive FA concentration, analogous studies on the influence of the concentration were carried out for aqueous solutions of sodium formate ( $NaHCO_2$ ). The pH value of  $NaHCO_2$  at  $10^{-2}$  and 1 M was about neutral in the both cases. An increase in the temporal  $H_2$  evolution plot upon increasing  $NaHCO_2$  concentration in the  $10^{-2}$  to 1 M was observed (Table 2). Accordingly, it is proposed that the MIP-177-LT structure is suitable to adsorb and recognize formate species, rather than FA. Adsorption of  $HCO_2^-$  on the *imprinting* active sites results in an enhanced photocatalytic  $H_2$  evolution.

Table 2. Photocatalytic H<sub>2</sub> release from sodium formate (NaHCO<sub>2</sub>) as a function of the concentration. *Reaction conditions: FA concentration 10<sup>-3</sup> M, photocatalyst 10 mg, solution volume 15 mL, 300 W Xe lamp through Pyrex, room temperature, reaction time 2 h.*

Time	H <sub>2</sub> release (μmol × g <sub>photocatalyst</sub> <sup>-1</sup> )	
	NaHCO <sub>2</sub> concentration 10 <sup>-2</sup> M	NaHCO <sub>2</sub> concentration 1 M
30	120	280
60	324	645
90	430	916
120	870	1250

Now, when using aqueous FA solution and according to the equilibrium constant, formate should also be present when the concentration of FA in aqueous solution is 10<sup>-2</sup> M and it is able to compete for the MIP-177 sites at this concentration. In contrast, the formate concentration becomes negligible compared to that of FA as the concentration of FA

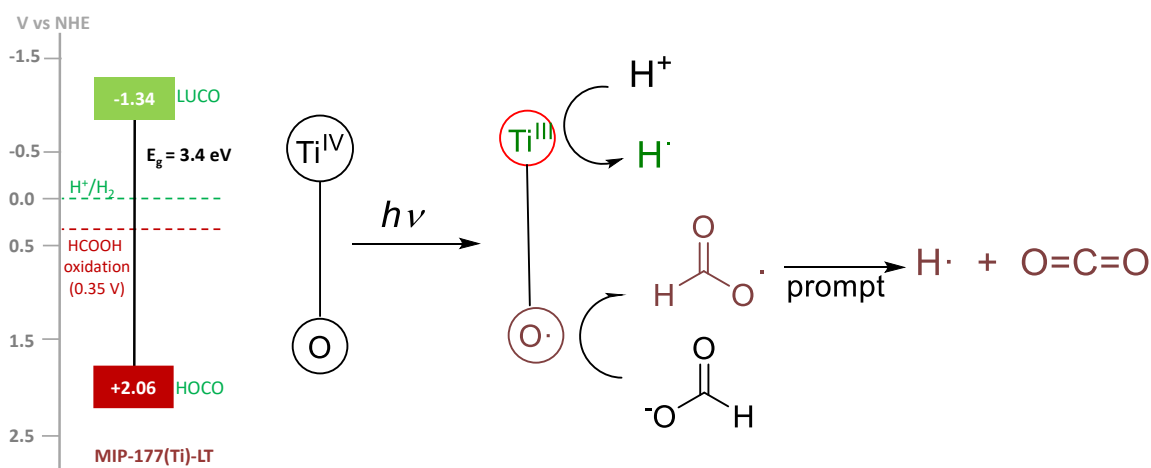
increases to 1 M. In addition, FA undergoes a strong association with the formation of FA dimers (eq. 3) at high concentration as observed in  $^1\text{H}$  NMR spectroscopy.<sup>[54]</sup> These two facts, the decrease in  $\text{HCO}_2^-$  concentration relative to FA concentration and FA dimer association, are proposed to be responsible for the unexpectedly lower observed photocatalytic activity of MIP-177 as the FA concentration increases. Therefore, in agreement with the structure of MIP-177-LT these measurements clearly reveal that it is formate the real species that is undergoing decomposition by the imprinted adjacent bi Ti sites. The bidentate bridging of formate according to Fig. 1 justifies also the absence of CO formation that occur for monodentate FA bridging.<sup>[6]</sup>



#### *Reaction mechanism.*

It is proposed that light absorption generates a transient state of charge separation resulting in electrons located at  $\text{Ti}^{\text{IV}}$  and holes in oxygen atoms of the clusters and/or the mdip carboxylates. These holes at  $\text{Ti}^{\text{III}}$  then abstract one electron from formate promoting decarboxylation of attached  $\text{HCO}_2^-$  radical intermediate, evolving  $\text{CO}_2$  and the formation of a surface H atom that will form a  $\text{H}_2$  molecule, with H atoms also formed by reduction of  $\text{H}^+$  by photogenerated electrons. Scheme 1 summarizes the proposal indicating the energy of

the lowest unoccupied and highest occupied crystal orbitals (LUCO and HOCO) in comparison to the potential of the  $\text{H}^+/\text{H}_2$  and  $\text{HCO}_2\text{H}/\text{CO}_2$  redox pairs. The main novelty of MIP-177-LT respect to the other two MOFs included in Table 1 is the presence of formate-imprinted sites in the structure that should favor adsorption of formates at the active site where holes are formed, thus increasing the efficiency of the process.



Scheme 1. Proposed reaction mechanism. Upon light absorption, an electron migrates by ligand-to-metal photoinduced charge transfer to the  $\text{Ti}^{\text{IV}}$ . Photogenerated electrons on  $\text{Ti}^{\text{III}}$  produce H atoms and photogenerated holes produce formate radicals that decompose to  $\text{CO}_2$  and H atoms.

To provide some support to this proposal, photocatalytic formate decomposition was performed in the presence of quenchers. Table S3 provides a summary of the quenching study. In this way, performing the photocatalytic formic acid decomposition in the presence of  $10^{-3}$  M of cerium ammonium nitrate results in a significant diminution of the amount of evolved  $\text{H}_2$  to about one third of the volume in the absence of  $\text{Ce}(\text{NH}_4)_2(\text{NO}_3)_6$ , while  $\text{CO}_2$  evolution was enhanced somewhat from 701 to



794  $\mu\text{mol} \times g_{\text{photocatalyst}}$  at 2 h reaction time. This observation is compatible with the mechanistic proposal, holes being consumed by formates evolving  $\text{CO}_2$ , while photogenerated electrons convert  $\text{Ce}^{\text{IV}}$  into  $\text{Ce}^{\text{III}}$ , thwarting in part  $\text{H}_2$  evolution that becomes unbalanced.

In contrast, all the attempts to stop or diminish  $\text{CO}_2$  evolution in MIP-177-LT as reference photocatalyst by using hole quenchers such as hydrogensulfite or hydrogen sulfide were unsuccessful (Table S4), probably reflecting the preferential selective formate adsorption on the Ti atoms respect to the quenchers.

#### *Molecular insights into the reaction mechanism*

Density functional theory (DFT) calculations implementing D3 dispersion correction (see supporting information) were further performed to shed light on the catalytic reaction mechanism and to understand the electronic and structural origins of the outstanding performance exhibited by MIP-177(Ti)-LT. Herein, a representative  $\text{Ti}_{12}\text{O}_{15}$  cluster model was cleaved from the periodic MOF structure integrating an unsaturated  $\text{Ti}^{\text{IV}}/\text{Ti}^{\text{III}}$  pair to account for the light-induced switching of one active site from  $\text{Ti}^{\text{IV}}$  to  $\text{Ti}^{\text{III}}$  as revealed experimentally and in line with previously reported Ti-MOFs.<sup>[55, 56]</sup> The first step of the reaction, i.e. chemisorption  $\text{HCOOH}$  throughout this Ti active site, is associated with an adsorption energy of -0.79 eV and Ti-O( $\text{HCOOH}$ ) distances of 2.65 Å ( $\text{Ti}^{\text{III}}$ ) and 2.61 Å ( $\text{Ti}^{\text{IV}}$ ) (Table S5) that suggests a favorable formation of this initial state, although without leading to a highly stable state that would be detrimental to proceed the following steps of the

mechanism. The calculated Gibbs-free energy profile for the dehydrogenation of \*HCOOH through the \*HCOO (formate) pathway was further explored (Fig. 5a). The adsorbed \*HCOOH molecule undergoes O–H bond cleavage to form \*HCOO\* and \*H first. At this step, the released H is coordinated to the  $\mu_0$  site, while O of \*HCOO\* still bonds to the Ti site. Then, \*HCOO undergoes a reorientation and the C-H bond breaks to form CO<sub>2</sub>.

For comparison, the TiO<sub>2</sub> (110) as benchmark photocatalyst was also computationally explored. We first calculated that the adsorption energy of HCOOH (-1.49 eV) on TiO<sub>2</sub> (110) is much higher than that calculated for MIP-177(Ti)-LT (-0.79 eV) in line with substantially shorter Ti-O(HCOOH) distances (2.10 Å and 2.18 Å vs 2.65 Å and 2.61 Å for MIP-177(Ti)-LT) (details shown in Table S5). The adsorption of \*HCOO is also more energetics on TiO<sub>2</sub> (110) surface than that of MIP-177(Ti)-LT (energy difference: 0.76 eV), which makes the cleavage of the C–H bond from \*HCOO much less thermodynamically preferable on TiO<sub>2</sub> ( $\Delta G=1.34$  eV) compared to MIP-177(Ti)-LT ( $\Delta G=0.35$  eV) as revealed in Fig. 5a. The local environment of Ti<sub>12</sub>O<sub>15</sub> inorganic node of MIP-177(Ti)-LT combined with its structural adaptability towards guest adsorption (see the guest-induced structure relaxation in Fig. S7 and Table S5) is a key to offer an optimum energetics for the coordination of \*HCOOH and \*HCOO to promote an effective catalytic activity according to the Sabatier principle.<sup>[57]</sup> The results of this calculation comparing the models for MIP-177-LT and TiO<sub>2</sub> agree well with the previously measured much higher activation energy value of 107.0 kJ × mol<sup>-1</sup> experimentally determined for TiO<sub>2</sub> in comparison to the 57.5 kJ × mol<sup>-1</sup> value for MIP-177-LT.

According to the Gibbs-free energy profile, the C-H cleavage of \*HCOO is the key step for H<sub>2</sub> release reaction. We analyzed the crystal orbital Hamilton populations (COHP) for \*HCOO adsorption configuration and we found that the interaction between \*HCOO and MIP-177(Ti)-LT comes from the anti-bonding between O of \*HCOO and Ti of MIP-177(Ti)-LT (Fig. 5b). In addition, for MIP-177(Ti)-LT, the charge density difference analysis clearly showed that there is an accumulation of electrons on the Ti atom and depletion on the O atom (Fig. 5c). This electronic transfer is at the origin of the relative strong interaction between the Ti and O atoms, beneficial for the following transformation of electrons to the C atom, promoting the cleavage of C-H. The density of states (DOS) analysis (Fig. 5d) evidenced that the O-*p* states contribute to the lowest unoccupied molecular orbital (LUMO) which accept electrons, while Ti-*d* states contribute to the highest occupied molecular orbital (HOMO) which provide electrons. The same conclusion can be drawn from the analysis of the \*HCOOH adsorption configuration (Fig. S8). This whole analysis supports that the light-induced Ti<sup>III</sup> plays a critical role in the whole photocatalytic FA decomposition of MIP-177(Ti)-LT.

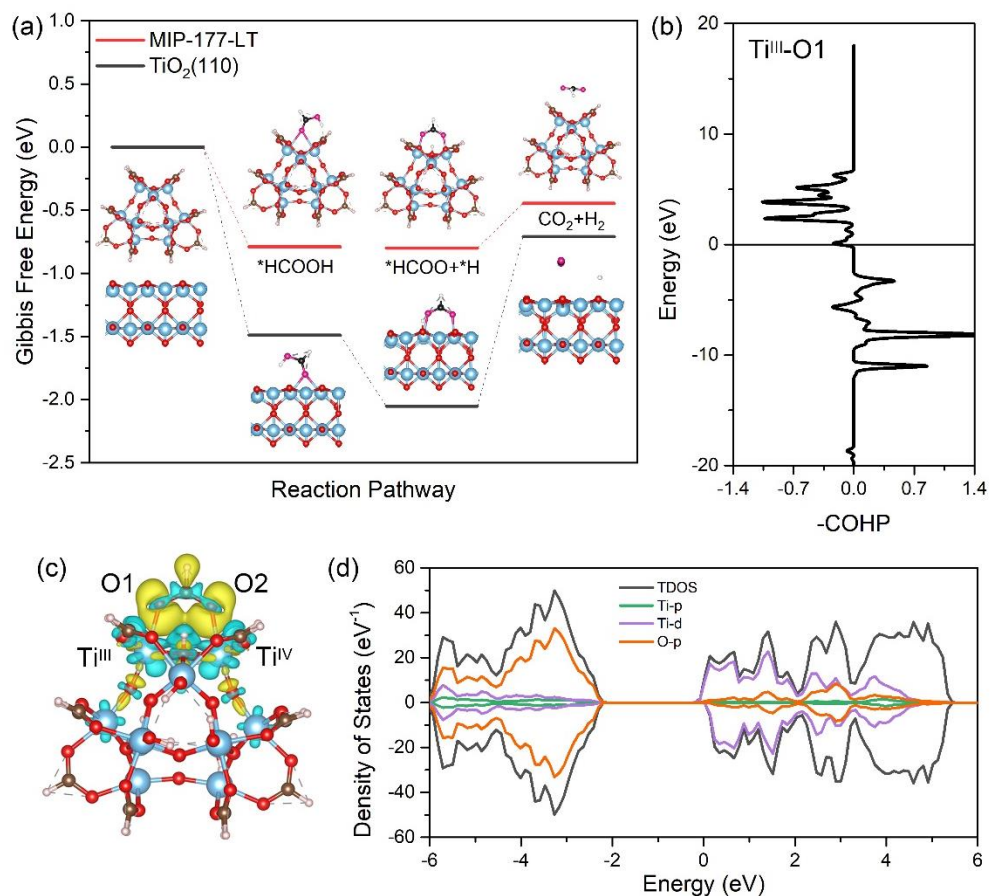


Fig. 5. (a) Gibbs free energy profile for the conversion  $\text{HCOOH}$  into  $\text{H}_2$  and  $\text{CO}_2$  simulated for MIP-177(Ti)-LT and  $\text{TiO}_2(110)$ . The total free energy of MIP-177(Ti)-LT and  $\text{TiO}_2$  models with gas-phase  $\text{HCOOH}$  molecule was set as the zero point in the energy profile. The color scheme for FA: O, pink; H, white; C, black; The color scheme for catalysts: Ti, blue; O, red; H: light pink. (b) COHP analysis of  $\text{*HCOO}$  on MIP-177-LT for  $\text{Ti}^{\text{III}}$  adsorption site. Positive and negative values of  $-\text{COHP}$  correspond to bonding and antibonding interactions. (c) Charge density difference of  $\text{*HCOO}$  on MIP-177(Ti)-LT cluster model. Yellow and blue lobes refer to electron accumulation and depletion regions. (d) Total and projected Density of States (DOS) of  $\text{*HCOO}$  on MIP-177(Ti)-LT cluster model.

### Photo response of MIP-177-LT

Further studies were aimed at determining the chromophores responsible for the photodecarboxylation by studying the influence of the irradiation wavelength in H<sub>2</sub> release from FA using MIP-177-LT as photocatalyst. The results are presented in Fig. 6. It can be seen that irradiation in the deep UV at 238 nm exhibits a high apparent quantum yield of 22 %. This remarkable quantum yield decreases as the irradiation wavelength becomes longer. At 300 nm, the apparent quantum yield is 0.5 %. This dependency of the photocatalytic activity with the wavelength indicates that direct excitation of Ti←O ligand-to-metal charge transfer band of Ti<sub>12</sub>O<sub>15</sub> clusters that should have an absorption band at 240 nm is the most efficient photophysical process to promote FA decarboxylation and H<sub>2</sub> release. [58, 59] Excitation at the localized organic mdip linker with absorption extending to 274 and 300 nm can also promote H<sub>2</sub> evolution through a Ti<sub>12</sub>O<sub>15</sub>←mdip ligand to metal charge transfer,[56] but with much less efficiency. This lesser efficiency indicates the incomplete quenching of localized mdip excitons by the Ti<sub>12</sub>O<sub>15</sub> cluster, probably because other deactivation pathways are available to the ligand excited state including radiationless decay through conformational phenyl ring rotation or emissive photoluminescence.

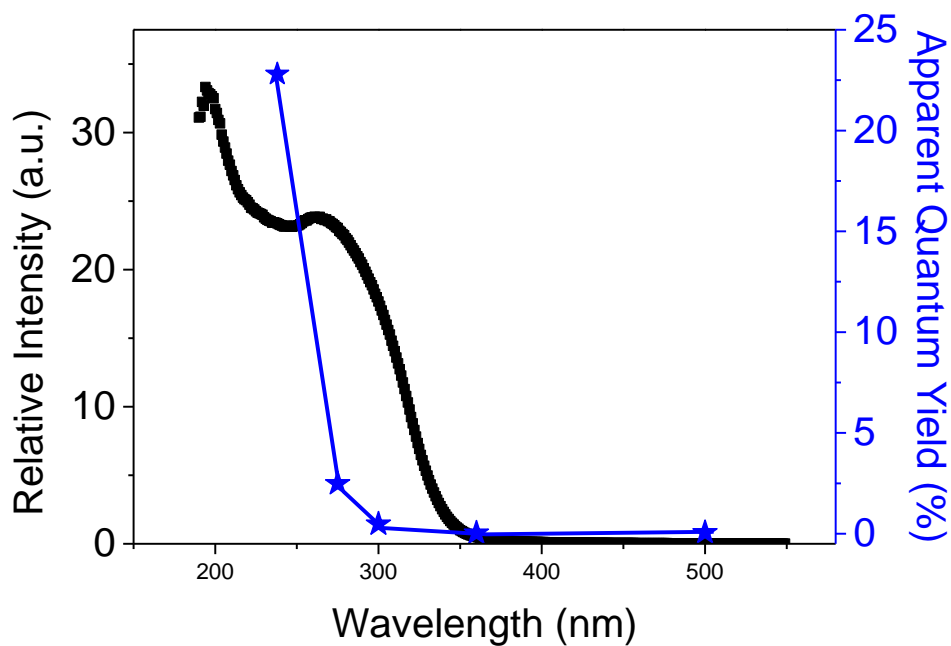


Fig. 6. Photoresponse MIP-177-LT for FA decarboxylation at different wavelengths (left axis) compared with the diffuse reflectance UV-Vis absorption spectrum for MIP-177-LT.

Photoresponse in the visible, although existing in MIP-177-LT, probably due to the action of structural defects or impurities, is orders of magnitude lower than in the UV. In fact, one of the improvements to increase photocatalytic activity of MIP-177-LT could be extending its photoresponse towards longer wavelengths by appropriate design of mixed metal or mixed ligand MIP-177 following reported strategies.

#### Scope.

Photocatalytic decarboxylation is a general reaction that has gained renewed interest as a way to obtain hydrocarbon fuels from biomass-derived aliphatic carboxylic

acids.<sup>[60, 61]</sup> As FA, other carboxylic acids can undergo photocatalytic decarboxylation to form the corresponding alkyl radicals that can abstract one hydrogen from the solvent, dimerize or undergo trapping after consecutive reactions.<sup>[60, 62, 63]</sup> It was of interest to determine, whether or not the formate-imprinted photocatalytic site of MIP-177-LT can also promote photodecarboxylation of other carboxylic acids with similar high activity. Therefore, besides FA decomposition, the photocatalytic activity of MIP-177-LT was also assessed in the photocatalytic decarboxylation of acetic, propionic and methacrylic acids.

As expected, all the tested aliphatic carboxylic acids undergo photodecarboxylation promoted by MIP-177-LT. The main product was CO<sub>2</sub>, accompanied by much lesser amounts of H<sub>2</sub> and light alkanes. The results are presented in Table 3. As it can be seen there, acetic acid at 10<sup>-3</sup> M concentration undergoes a complete photocatalytic decarboxylation after 16 h irradiation time. The initial evolution of H<sub>2</sub> during the irradiation indicates that formate groups present in MIP-177-LT are undergoing photodecarboxylation in the first stages, before observing acetic acid decarboxylation. Interestingly, a second use of the MIP-177-LT shows a considerable deactivation degree of about 90 % that further decreases to a residual 5 % of the initial activity in the third use. This behavior contrasts to the previously commented growth in MIP-177-LT catalytic activity using FA and indicates the poisoning of the active sites by some blocking by-products. The fact that methane is not evolved in the expected stoichiometric amounts respect to CO<sub>2</sub> suggest that some by product such as methoxy groups could be blocking the sites.

Propanoic acid also undergoes photodecarboxylation in a considerable extent after 2 h of 300 W Xe lamp irradiation (Table 3) and undergoes deactivation in the second use to

a value corresponding to only about 20 % of the activity of the fresh MIP-177-LT. Although the origin of deactivation deserves a deeper study, PXRD of the deactivated MIP-177-LT after its use as photocatalyst shows that the crystallinity of the samples has been preserved, indicating that MIP-177-LT decomposition is not the reason of the loss of photocatalytic activity.

Similar trends were also observed for the photocatalytic decomposition of methacrylic acid promoted by MIP-177-LT, i.e., evolution of CO<sub>2</sub> without being accompanied of similar proportions of other organic hydrocarbons and considerable deactivation upon reuse.

Although further studies are necessary to understand the photocatalytic data and performance of MIL-177-LT for acetic, propionic and methacrylic acid, the behavior with these carboxylic acids clearly contrasts with that of FA, thus reinforcing the importance of formate imprinting on the Ti<sub>12</sub>O<sub>15</sub> nodes on the photocatalytic H<sub>2</sub> release activity and stability.

Table 3. Products and H<sub>2</sub> evolution upon irradiation of carboxylic acids using MIP-177-LT as photocatalysts. Reaction conditions: 15 mL aqueous solution of 10<sup>-3</sup> M carboxylic acid, MIP-177-LT 10 mg, 300 W Xe lamp, reactor volume 51 mL, time 2 h.

Carboxylic acid	H <sub>2</sub> ( $\mu\text{mol} \times \text{g}_{\text{photocatalyst}}^{-1}$ )	CO <sub>2</sub> ( $\mu\text{mol} \times \text{g}_{\text{photocatalyst}}^{-1}$ )	Other



Acetic acid 16 h	1350	1405	CH <sub>4</sub>
Propionic acid 2 h	1487	922	CH <sub>4</sub> , CH <sub>3</sub> CH <sub>3</sub>
Methacrylic acid	1410	1490	CH <sub>4</sub> , CH <sub>3</sub> -CH=CH <sub>2</sub>

### Conclusions.

It has been shown that Ti-MOF MIP-177-LT combines several properties that makes this material highly active for the photocatalytic H<sub>2</sub> release from FA, specially the presence of accessible formate-imprinted active sites in equatorial Ti atoms and its structural robustness in strong acid media. These unique features led to a FA decomposition activity over one order of magnitude superior to the ones of the benchmark MOF photocatalysts MIL-125(Ti) and UiO-66(Zr) or over 30 times that of TiO<sub>2</sub> P25, reaching an apparent quantum yield as high as 22 % in the UV. Noteworthy, the FA photocatalytic decomposition rate of the fresh MIP-177-LT increases upon irradiation and is disfavored at high FA concentrations, facts that are related to the preference of the material for formate respect to its acid form. Acid washings has a beneficial influence on the photocatalytic activity of MIP-177-LT-AT by removing impurities and releasing the active centers, reaching a maximum TOF value of 0.46 h<sup>-1</sup>. Quenching studies and DFT calculations support that H<sub>2</sub> consumes photogenerated electrons, but CO<sub>2</sub> evolution could not be quenched by strong electron donors indicating the high selectivity of the active sites for formate coordination. Considering the advantage

of light over heat for instantaneous on-off control of H<sub>2</sub> release, the present results open the way for efficient MOF photocatalysts by design based on earth abundant and affordable elements.

### Acknowledgements.

Financial support by the Spanish Ministerio de Ciencia e Innovación (PID2021-126071OB-C21 and Severo Ochoa) and Generalitat Valenciana (Prometeo 2017/083) is gratefully acknowledged.

### References.

- [1] Z. Abdin, A. Zafaranloo, A. Rafiee, W. Mérida, W. Lipiński, K. R. Khalilpour, *Renewable and sustainable energy reviews* **2020**, *120*, 109620.
- [2] S. Sharma, S. K. Ghoshal, *Renewable and sustainable energy reviews* **2015**, *43*, 1151-8.
- [3] T. He, Q. Pei, P. Chen, *Journal of energy chemistry* **2015**, *24*, 587-94.
- [4] D. Teichmann, W. Arlt, P. Wasserscheid, R. Freymann, *Energy & Environmental Science* **2011**, *4*, 2767-73.
- [5] M. Grasmann, G. Laurenczy, *Energy & Environmental Science* **2012**, *5*, 8171-81.
- [6] K. Tedsree, T. Li, S. Jones, C. W. A. Chan, K. M. K. Yu, P. A. J. Bagot, E. A. Marquis, G. D. W. Smith, S. C. E. Tsang, *Nature Nanotechnology* **2011**, *6*, 302-7.
- [7] S. Fukuzumi, T. Kobayashi, T. Suenobu, *ChemSusChem: Chemistry & Sustainability Energy & Materials* **2008**, *1*, 827-34.
- [8] Y. Himeda, *Green Chemistry* **2009**, *11*, 2018-22.
- [9] S.-M. Lu, Z. Wang, J. Wang, J. Li, C. Li, *Green Chemistry* **2018**, *20*, 1835-40.
- [10] Z. L. Wang, J. M. Yan, Y. Ping, H. L. Wang, W. T. Zheng, Q. Jiang, *Angewandte Chemie* **2013**, *125*, 4502-5.
- [11] Q. Zhang, Q. Mao, Y. Zhou, L. Zou, D. Zhu, Y. Huang, H. Gao, X. Luo, Y. Mao, Z. Liang, *ACS Sustainable Chemistry & Engineering* **2022**, *10*, 4599-609.
- [12] D. Mellmann, E. Barsch, M. Bauer, K. Grabow, A. Boddien, A. Kammer, P. Sponholz, U. Bentrup, R. Jackstell, H. Junge, *Chemistry—A European Journal* **2014**, *20*, 13589-602.
- [13] D. Mellmann, P. Sponholz, H. Junge, M. Beller, *Chemical Society Reviews* **2016**, *45*, 3954-88.
- [14] A. Léval, A. Agapova, C. Steinlechner, E. Alberico, H. Junge, M. Beller, *Green Chemistry* **2020**, *22*, 913-20.
- [15] N. Onishi, G. Laurenczy, M. Beller, Y. Himeda, *Coordination Chemistry Reviews* **2018**, *373*, 317-32.
- [16] V. Singh, R. Singh, *Corrosion Science* **1995**, *37*, 1399-410.

- [17] K. Grubel, H. Jeong, C. W. Yoon, T. Autrey, *Journal of Energy Chemistry* **2020**, *41*, 216-24.
- [18] K. Sordakis, A. F. Dalebrook, G. Laurenczy, *ChemCatChem* **2015**, *7*, 2332-9.
- [19] J. r. Eppinger, K.-W. Huang, *ACS Energy Letters* **2017**, *2*, 188-95.
- [20] B. M. Besancon, V. Hasanov, R. Imbault-Lastapis, R. Benesch, M. Barrio, M. J. Mølnvik, *International Journal of Hydrogen Energy* **2009**, *34*, 2350-60.
- [21] M. Navlani-García, D. Salinas-Torres, K. Mori, Y. Kuwahara, H. Yamashita, *Heterogeneous Photocatalysis* **2020**, 193-223.
- [22] H. J. Yun, H. Lee, J. B. Joo, W. Kim, J. Yi, *The Journal of Physical Chemistry C* **2009**, *113*, 3050-5.
- [23] Z. Zhang, S.-W. Cao, Y. Liao, C. Xue, *Applied Catalysis B: Environmental* **2015**, *162*, 204-9.
- [24] Y. Ji, Y. Luo, *Journal of Power Sources* **2016**, *306*, 208-12.
- [25] A. Gazsi, G. Schubert, P. Pusztai, F. Solymosi, *International journal of hydrogen energy* **2013**, *38*, 7756-66.
- [26] C. Tao, W. Guopeng, F. Zhaochi, H. Gengshen, S. Weiguang, Y. Pinliang, L. Can, *Chinese Journal of Catalysis* **2008**, *29*, 105-7.
- [27] K. L. Miller, C. W. Lee, J. L. Falconer, J. W. Medlin, *Journal of Catalysis* **2010**, *275*, 294-9.
- [28] B. Wu, J. Lee, S. Mubeen, Y. S. Jun, G. D. Stucky, M. Moskovits, *Advanced Optical Materials* **2016**, *4*, 1041-6.
- [29] I. Willner, Z. Goren, *Journal of the Chemical Society, Chemical Communications* **1986**, 172-3.
- [30] S. Cao, Y. Chen, H. Wang, J. Chen, X. Shi, H. Li, P. Cheng, X. Liu, M. Liu, L. Piao, *Joule* **2018**, *2*, 549-57.
- [31] R. Zhu, F. Tian, R. Yang, J. He, J. Zhong, B. Chen, *Renewable Energy* **2019**, *139*, 22-7.
- [32] M. Hamandi, G. Berhault, C. Guillard, H. Kochkar, *Applied Catalysis B: Environmental* **2017**, *209*, 203-13.
- [33] Q. Zhang, C.-F. Lin, Y. H. Jing, C.-T. Chang, *Journal of the Air & Waste Management Association* **2014**, *64*, 578-85.
- [34] M. Hamandi, G. Berhault, C. Guillard, H. Kochkar, *Molecular Catalysis* **2017**, *432*, 125-30.
- [35] C. Wan, L. Zhou, L. Sun, L. Xu, D.-g. Cheng, F. Chen, X. Zhan, Y. Yang, *Chemical Engineering Journal* **2020**, *396*, 125229.
- [36] A. Dhakshinamoorthy, Z. Li, H. Garcia, *Chemical Society Reviews* **2018**, *47*, 8134-72.
- [37] A. Dhakshinamoorthy, A. M. Asiri, H. Garcia, *Angewandte Chemie International Edition* **2016**, *55*, 5414-45.
- [38] X. Deng, Z. Li, H. García, *Chemistry—A European Journal* **2017**, *23*, 11189-209.
- [39] M. Zeng, Z. Chai, X. Deng, Q. Li, S. Feng, J. Wang, D. Xu, *Nano Research* **2016**, *9*, 2729-34.
- [40] M. Wen, K. Mori, Y. Kuwahara, H. Yamashita, *ACS Energy Letters* **2017**, *2*, 1-7.
- [41] M. Zhang, W. Lin, L. Ma, Y. Pi, T. Wang, *Chemical Communications* **2022**, *58*, 7140-3.
- [42] D. Jiang, C. Huang, J. Zhu, P. Wang, Z. Liu, D. Fang, *Coordination Chemistry Reviews* **2021**, *444*, 214064.
- [43] N. Stock, S. Biswas, *Chemical reviews* **2012**, *112*, 933-69.
- [44] S. A. Younis, E. E. Kwon, M. Qasim, K.-H. Kim, T. Kim, D. Kukkar, X. Dou, I. Ali, *Progress in Energy and Combustion Science* **2020**, *81*, 100870.
- [45] M. Ghorbanloo, V. Safarifard, A. Morsali, *New Journal of Chemistry* **2017**, *41*, 3957-65.
- [46] J. Sun, J. Wan, Y. Wang, Z. Yan, Y. Ma, S. Ding, M. Tang, Y. Xie, *Journal of Hazardous Materials* **2022**, *429*, 128299.
- [47] G. Wißmann, A. Schaate, S. Lilienthal, I. Bremer, A. M. Schneider, P. Behrens, *Microporous and Mesoporous Materials* **2012**, *152*, 64-70.

- [48] H. Assi, G. Mouchaham, N. Steunou, T. Devic, C. Serre, *Chemical Society Reviews* **2017**, *46*, 3431-52.
- [49] S. Wang, T. Kitao, N. Guillou, M. Wahiduzzaman, C. Martineau-Corcus, F. Nouar, A. Tissot, L. Binet, N. Ramsahye, S. Devautour-Vinot, S. Kitagawa, S. Seki, Y. Tsutsui, V. Briois, N. Steunou, G. Maurin, T. Uemura, C. Serre, *Nature communications* **2018**, *9*, 1660-.
- [50] S. Nandi, S. Wang, M. Wahiduzzaman, V. Yadav, K. Taksande, G. Maurin, C. Serre, S. Devautour-Vinot, *ACS Applied Materials & Interfaces* **2021**, *13*, 20194-200.
- [51] R. V. Pinto, S. Wang, S. R. Tavares, J. Pires, F. Antunes, A. Vimont, G. Clet, M. Daturi, G. Maurin, C. Serre, *Angewandte Chemie International Edition* **2020**, *59*, 5135-43.
- [52] D. Mateo, A. Santiago - Portillo, J. Albero, S. Navalón, M. Alvaro, H. García, *Angewandte Chemie* **2019**, *131*, 18007-12.
- [53] M.-Y. Qi, M. Conte, M. Anpo, Z.-R. Tang, Y.-J. Xu, *Chemical Reviews* **2021**.
- [54] W. Reutemann, H. Kieczka, *Ullmann's encyclopedia of industrial chemistry* **2011**, *1*.
- [55] M. de Miguel, F. Ragon, T. Devic, C. Serre, P. Horcajada, H. García, *ChemPhysChem* **2012**, *13*, 3651-4.
- [56] A. Santiago Portillo, H. G. Baldoví, M. T. Garcia Fernandez, S. Navalon, P. Atienzar, B. Ferrer, M. Alvaro, H. Garcia, Z. Li, *The Journal of Physical Chemistry C* **2017**, *121*, 7015-24.
- [57]
- [58] A. Dhakshinamoorthy, S. Navalon, A. Corma, H. Garcia, *Energy & Environmental Science* **2012**, *5*, 9217-33.
- [59] C. Aprile, A. Corma, H. Garcia, *Physical Chemistry Chemical Physics* **2008**, *10*, 769-83.
- [60] D. Budac, P. Wan, *Journal of Photochemistry and Photobiology A: Chemistry* **1992**, *67*, 135-66.
- [61] X. Du, Y. Peng, J. Albero, D. Li, C. Hu, H. García, *ChemSusChem* **2022**, *15*, e202102107.
- [62] J. Schwarz, B. König, *Green Chemistry* **2018**, *20*, 323-61.
- [63] J. Shi, T. Yuan, M. Zheng, X. Wang, *ACS Catalysis* **2021**, *11*, 3040-7.